

Data-driven ballast layer degradation identification and maintenance decision based on track geometry irregularities

Zhao, Wenbo; Qiang, Weile; Yang, Fei; Jing, Guoqing; Guo, Yunlong

DOI

[10.1080/23248378.2023.2228802](https://doi.org/10.1080/23248378.2023.2228802)

Publication date

2023

Document Version

Final published version

Published in

International Journal of Rail Transportation

Citation (APA)

Zhao, W., Qiang, W., Yang, F., Jing, G., & Guo, Y. (2023). Data-driven ballast layer degradation identification and maintenance decision based on track geometry irregularities. *International Journal of Rail Transportation*, 12(4), 581-603. <https://doi.org/10.1080/23248378.2023.2228802>

Important note

To cite this publication, please use the final published version (if applicable).
Please check the document version above.

Copyright

Other than for strictly personal use, it is not permitted to download, forward or distribute the text or part of it, without the consent of the author(s) and/or copyright holder(s), unless the work is under an open content license such as Creative Commons.

Takedown policy

Please contact us and provide details if you believe this document breaches copyrights.
We will remove access to the work immediately and investigate your claim.



Data-driven ballast layer degradation identification and maintenance decision based on track geometry irregularities

Wenbo Zhao, Weile Qiang, Fei Yang, Guoqing Jing & Yunlong Guo

To cite this article: Wenbo Zhao, Weile Qiang, Fei Yang, Guoqing Jing & Yunlong Guo (2023): Data-driven ballast layer degradation identification and maintenance decision based on track geometry irregularities, International Journal of Rail Transportation, DOI: [10.1080/23248378.2023.2228802](https://doi.org/10.1080/23248378.2023.2228802)

To link to this article: <https://doi.org/10.1080/23248378.2023.2228802>



© 2023 The Author(s). Published by Informa UK Limited, trading as Taylor & Francis Group.



Published online: 25 Jun 2023.



[Submit your article to this journal](#)



Article views: 131



[View related articles](#)



[View Crossmark data](#)



Data-driven ballast layer degradation identification and maintenance decision based on track geometry irregularities

Wenbo Zhao^a, Weile Qiang^a, Fei Yang^a, Guoqing Jing^b and Yunlong Guo^{b,c}

^aInfrastructure Inspection Research Institute, China Academy of Railway Sciences Co., Ltd, Beijing, China; ^bSchool of Civil Engineering, Beijing Jiaotong University, Beijing, China; ^cFaculty of Civil Engineering and Geosciences, Delft University of Technology, Delft, Netherlands

ABSTRACT

Ballast layer defects are the primary cause for rapid track geometry degradation. Detecting these defects in real-time during track inspections is urgently needed to ensure safe train operations. To achieve this, an indicator, the track degradation rate (TDR) was proposed. This rate is calculated using track geometry inspection data to locate and predict railway-line sections with ballast layer defects. The TDR is determined by the monthly standard deviation of the rail longitudinal level, which is one aspect of track geometry. The Ballast Layer Health Classification (BLHC) is designed by assessing the two successive TDRs before and after track geometry maintenance actions. The BLHC is used to categorize the conditions of the ballast layer, including normal periodic deterioration, abrupt deterioration, effective maintenance, rising deterioration, and severe deterioration. Both the TDR and BLHC were validated through field assessments of ballast layer conditions, where the two indicators were found to be effective in revealing defects. The results indicate that the TDR is sensitive to ballast layer defects, while the BLHC can quickly identify the location of these defects. Consequently, the BLHC can provide real-time guidance for ballast layer maintenance.

ARTICLE HISTORY

Received 4 January 2023

Revised 16 June 2023

Accepted 19 June 2023



KEYWORDS

Ballast inspection; data science; maintenance; ballast degradation; track geometry; track irregularity

1. Introduction

Ballasted tracks, as one conventional railway infrastructure, can offer significant benefits compared to other types of tracks, including low construction costs, rapid construction, and ease of maintenance. As such, ballasted tracks are widely used in various types of rail transportation infrastructure globally [1]. An essential component of ballasted tracks is the ballast layer, which serves to secure the sleepers, transfer train loads to the subgrade, and provide some degree of drainage [2,3].

Despite its importance, the ballast layer is also regarded as one of the weakest parts of the track structure due to its discrete nature, which often leads to unpredictable defects [4,5]. Research has shown that ballast layer undergoes both vertical and lateral deformation when subjected to external loads, leading to track instability [6]. In particular, differential settlement of the ballast layer can directly impact the alignment of the track geometry (track height in the longitudinal direction), posing a serious threat to the safety of train operations [7].

CONTACT Yunlong Guo  yunlong.guo@tudelft.nl  Faculty of Civil Engineering and Geosciences, Delft University of Technology, Delft 2628CN, Netherlands

© 2023 The Author(s). Published by Informa UK Limited, trading as Taylor & Francis Group.

This is an Open Access article distributed under the terms of the Creative Commons Attribution-NonCommercial-NoDerivatives License (<http://creativecommons.org/licenses/by-nc-nd/4.0/>), which permits non-commercial re-use, distribution, and reproduction in any medium, provided the original work is properly cited, and is not altered, transformed, or built upon in any way. The terms on which this article has been published allow the posting of the Accepted Manuscript in a repository by the author(s) or with their consent.

As trains pass over the tracks, relative motions between ballast particles (also between ballast and sleeper) can result in particle abrasion and breakage [8]. The resulting fine particles, also known as ballast contamination or fouling, accumulate from the base of the ballast layer to its surface [9]. This process is especially problematic at the interface between the ballast and subgrade, where water tends to accumulate, leading to the formation of ‘ballast pockets’ that are difficult to inspect and maintain [10].

In addition, ballast particle degradation is the principal source of ballast fouling. According to a study [11], fouling caused by ballast particle degradation accounts for 70% of the total ballast layer fouling. More concerning is that in the interaction of water and fine particles, and with the inclusion of subgrade soil, the ballast layer can quickly lose its elasticity and permeability [12,13], eventually leading to an undesirable phenomenon, known as mud-pumping [14].

These ballast layer and ballast particle degradations not only impair the performance of the ballast layer but also contribute to rapid deterioration of other track components due to ballast degradation-caused impact loading. For example, this can lead to intensified rail–wheel interaction, hanging sleepers and lost fasteners [15,16]. Literature suggests that 50–70% of ballasted track defects stem from issues within the ballast layer [11]. This results in not only extremely high maintenance costs to restore ballast layer functionality but also impacts the safety of operations and passenger comfort.

To elaborate, defects in the ballast layer can reduce the layer’s bearing capacity by diminishing its shear strength and overall track elasticity [17,18]. Moreover, a fouled ballast layer can lead to issues such as poor drainage (resulting in mud-pumping) and frost heave during winter [19,20]. Most notably, uneven deformation, or differential settlement of the ballast layer, causes the tracks to endure the impact of train loads, which in turn accelerates the development of track geometry irregularity [21]. As train speeds increase, track geometry irregularities lead to more intense train–track interaction vibrations, causing track components to degrade more rapidly [22].

In order to mitigate the impact of ballast layer defects on the performance of ballasted tracks, the rapid detection of these defects and condition-based maintenance are urgently needed. Ballast layer inspection methods include manual visual inspection, track inspection vehicles (also known as inspection trains), and machine vision-based inspections.

- Manual visual inspection is a traditional method where obvious ballast layer defects, such as mud-pumping, are observed. Traditionally, the identification of ballast layer defects involves drilling and then sieving the obtained samples. However, this method is both destructive to the ballast layer and time-consuming.
- Machine vision-based inspection is a current area of intense research. Technologies used include ground penetrating radar (GPR), LiDAR, and InSAR [23–27]. While these methods have been used to identify ballast fouling, analysing the resultant image data is very time-consuming and requires experienced experts.
- Track inspection trains primarily measure track geometry, rail wear, and similar track condition indicators. However, they have not yet been successful in truly identifying the root cause of these track defects, particularly those arising from ballast layer defects [24].

Addressing these limitations, the proposed track geometry-based method is faster than both manual and machine vision inspections, as it can process data more rapidly, in real-time identifying the locations with ballast layer defects. Additionally, track inspection trains can initially locate the sections of railway lines with ballast layer defects, and then ground-penetrating radar (GPR) can be used to accurately analyse the cause of these defects (water content, layer thickness, mud-pumping, etc.).

Several studies have been conducted on analysing track geometry data. Below are some representative studies, with more relevant ones being available in [28–30].

- In [31], researchers measured the long-term track geometry and track stiffness of a heavy haul railway line. They confirmed the relationship between track stiffness and track geometry degradation rates.
- The study outlined in [32] shows that ballast layer settlement has an approximately positive relationship with track geometry irregularities. The influence of ballast layer deformation on track geometry irregularities becomes increasingly decisive with the prolonged service duration.
- Studies in [33,34] suggest that track geometry irregularities exhibit a linear deterioration trend between two adjacent maintenance actions. The progression of track geometry was predicted using linear regression models.
- In [35], an artificial neural network was used to predict the track geometry degradation rate. The study found a strong correlation between ballast layer degradation and the track geometry degradation rate.

The aforementioned studies suggest that the condition of the ballast layer (including defects and performance) can be strongly correlated with track geometry. However, very few studies have been conducted on locating ballast layer defects or conditions using track geometry data (e.g., data from inspection trains). The track geometry inspection train used in this study is shown in [Figure 1](#).

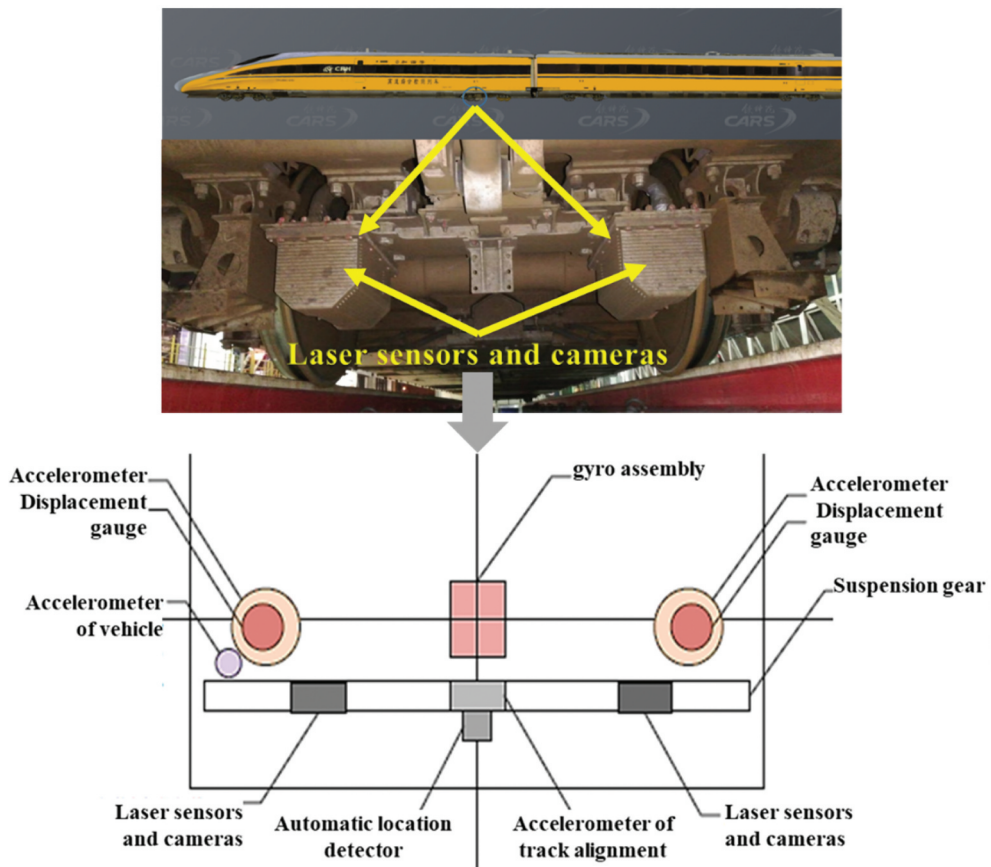


Figure 1. Inspection train of China academy of railway sciences.

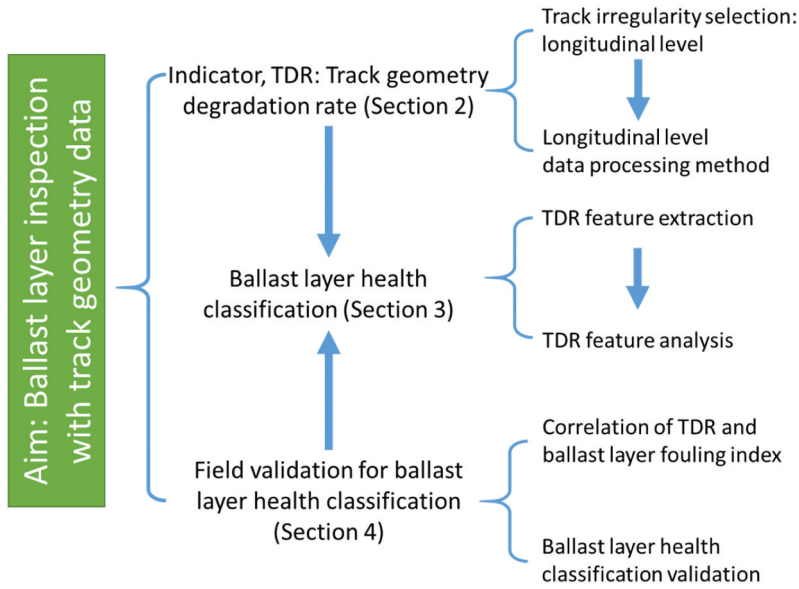


Figure 2. Structure of this paper: methodology and validation.

Therefore, this study concentrates on establishing a correlation between ballast layer defects and track geometry data. Furthermore, we validate this methodology by comparing the track geometry results with Ground Penetrating Radar (GPR) results and field observations. The primary contribution of this paper lies in the development of this methodology, which serves as our motivation.

In essence, with the development and application of mobile track inspection equipment (comprehensive inspection train), large amounts of track geometry data have been collected. This paper aims to leverage this data to identify railway-line sections with ballast layer defects, thereby providing a scientific basis for track maintenance. Specifically, we analysed consecutive track irregularity inspection data for a railway line section to derive the law of track geometry irregularity development. Based on this law, we used the track geometry deterioration rate to calculate a new indicator, the Track Degradation Rate (TDR), which can identify and predict ballast layer defects. The Ballast Layer Health Classification (BLHC) is derived based on TDR feature analysis, which is used to categorize the conditions of the ballast layer.

The results of this study can promptly identify, locate, and predict sections with ballast layer defects, thereby informing timely maintenance measures (such as tamping and renewal of the ballast layer) to prevent further deterioration. This can prolong the service life of the ballast layer and, consequently, the overall ballasted track. In conclusion, this study can provide technical support for the scientifically sound and economically efficient maintenance of ballasted tracks. The structure of this study is depicted in [Figure 2](#).

2. TRate (TDR) indicator

In this section, we will explain the reasoning behind choosing the longitudinal level (one index for track geometry). Subsequently, we will introduce the method for processing longitudinal level data. Finally, using the processed longitudinal level data, we will provide the method for calculating the Track Degradation Rate (TDR).

2.1. Track irregularity index selection

2.1.1. Track geometry irregularity calculation method

The objective of the method developed is to establish correlations between track geometry irregularities and ballast layer conditions. The first step in the method is identifying the most suitable index (presenting track geometry irregularity) to reflect ballast layer defects.

The track geometry data used in this paper was obtained from an inspection train developed by the China Academy of Railway Sciences (as depicted in Figure 1). This inspection train can measure various track geometry data used to calculate the Track Quality Index (TQI) and monitor train-track interactions.

We chose the longitudinal level, one type of track geometry, for calculating the track degradation rate (TDR). Also, the railway-line section length used for calculating the longitudinal level is less than 42 metres, as it has a good correlation with ballast layer conditions. Specifically, track geometry irregularity exhibits randomness because it arises from the superposition of simple harmonics at various frequencies and different phase angles. The formation and development of track irregularities are the results of these harmonics. The long-wave composition (longer than 42 metres) is primarily due to the deformation of the subgrade and foundation [36]. In contrast, the medium-short wave composition (shorter than 42 metres) arises from the deformation of the ballast layer.

Track quality evaluation is primarily based on a combination of two methods: local spot observation and railway-line section assessment. According to the European standard, track geometry irregularities include alignment, track gauge, longitudinal level, cross level, and twist [37]. Similarly, the Track Quality Index (TQI) is the standard indicator used in China's railways for evaluating overall track geometry quality. The TQI is calculated based on seven factors: longitudinal level (left rail and right rail), alignment (left rail and right rail), track gauge, cross level, and twist, as per Equations 1–4.

$$\bar{x}_i = \frac{1}{n} \sum_{j=1}^n x_{ij} \quad (1)$$

$$\sigma_i = \sqrt{\frac{1}{n} \sum_{j=1}^n (x_{ij} - \bar{x}_i)^2} \quad (2)$$

$$\sigma_i = \sqrt{\frac{1}{n} \sum_{j=1}^n (x_{ij} - \bar{x}_i)^2} \quad (3)$$

$$\text{TQI} = \sum_{i=1}^7 \sigma_i \quad (4)$$

In the Equations, x_{ij} is the measured track irregularity value (TQI factors) at the j -th sampling point of the i -th TQI factor; \bar{x}_i is the arithmetic mean of the i -th TQI factor; σ_i is the SD of the i -th TQI factor; n is the number of sampling points.

The standard deviation (SD) of each TQI factor reflects the dispersion degree of track irregularity within one line section. To accurately reflect the SD trends and precisely locate track geometry irregularities, the SD data are modified, and the effects can be found in Figure 3.

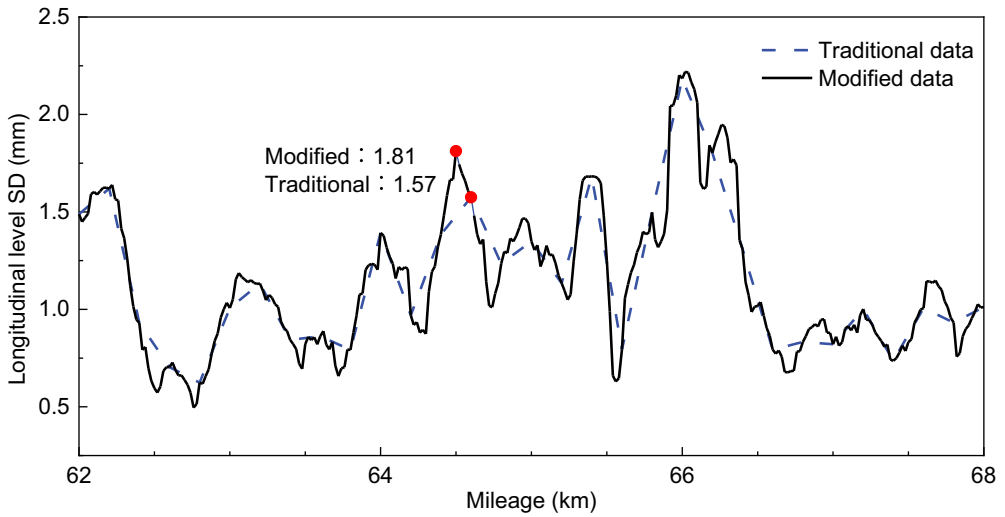


Figure 3. SD trends of longitudinal level as an example of all track quality index factors.

The SD is calculated for every 200 m length section. However, the SD sequence can omit some high amplitude values and may not accurately pinpoint the variations along the railway line (see Figure 3, traditional data). To more accurately locate track geometry irregularities, it is necessary to increase the sampling frequency. In this paper, we used a 20 m resampling rate. This means that every 20 m length section is used to calculate the SD of track irregularity, which can reflect SD trends more accurately and identify track irregularity sections with more precision (see Figure 3, modified data).

2.1.2. Correlation between track irregularity indices and ballast layer condition

According to field experiences, a poor ballast layer condition often correlates with poor track geometry, and the track is more likely to have a high Track Quality Index (TQI). Tracks with poor ballast layers require frequent tamping and stabilization and deteriorate at a relatively rapid rate [38].

The thickness of the clean ballast layer is a sensitive indicator reflecting the condition of the ballast layer [23]. This is because under cyclic loading, the ballast layer becomes fouled by various types of contamination. These contaminations accumulate at the base of the ballast layer, dividing it into clean and fouled layers [4]. The fouled ballast layer experiences an increase in cumulative deformation (settlement) [39], while a thick clean ballast layer provides sufficient elasticity and stability [40,41]. The thicknesses of the clean and dirty layers can be detected using ground penetrating radar. This inspection method was validated in our earlier study [42].

To obtain a statistical correlation between the TQI factors and the thickness of the clean ballast layer, we compared the inspection results of a railway line section using a scatter plot (Figure 4). Each point in the scatter plot represents the measured data in the same section. From the graph at row 4, columns 2 (Figure 4), it can be seen that the thickness of the clean layer shows a negative correlation with the longitudinal level, while there is no obvious correlation with other TQI factors.

Next, the Pearson correlation coefficient is used to analyse and quantify the correlation between the TQI factors (standard deviations) and the thickness of the clean ballast layer. The Pearson correlation coefficient is calculated as shown in Equation 5, and its resulting value ranges from -1 to

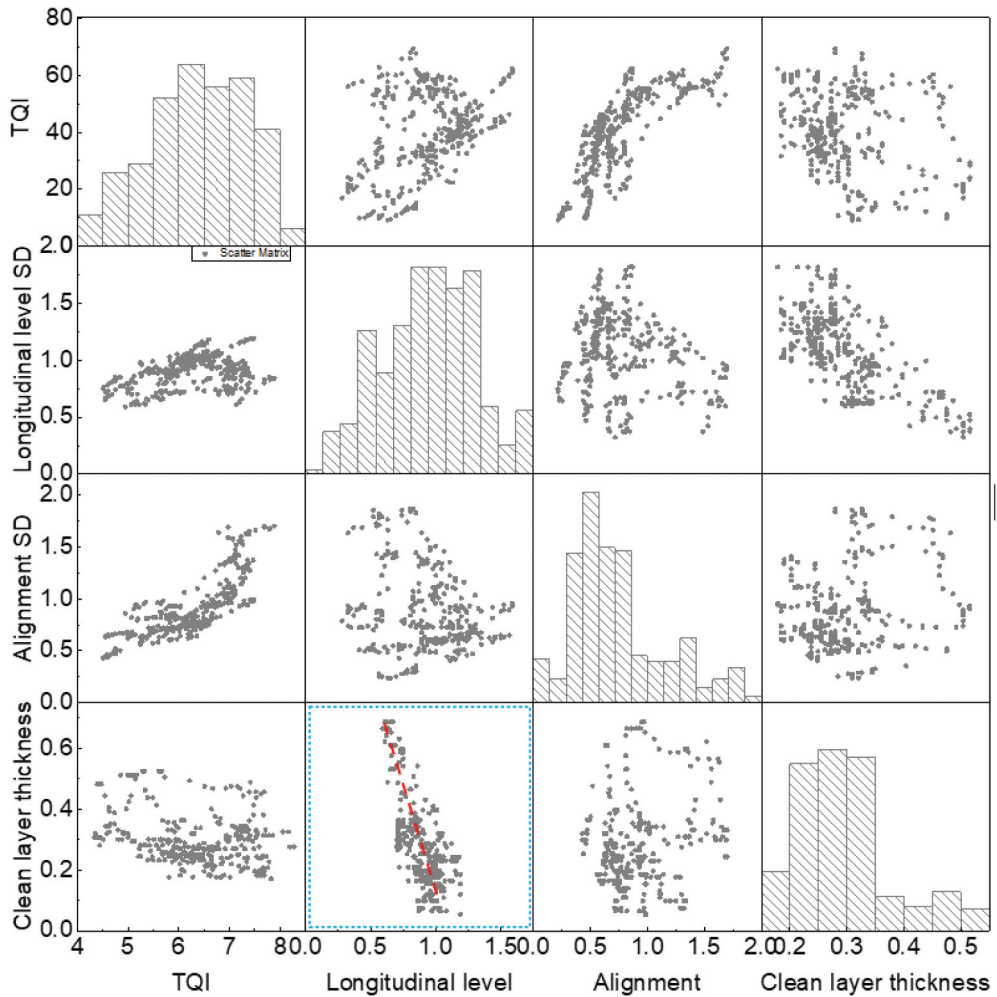


Figure 4. Correlation between TQI factors and thickness of clean ballast layer.

Table 1. Pearson correlation coefficient between TQI factors and thickness of clean ballast layer.

	TQI	Longitudinal level	Alignment	Track gauge	Cross level	Twist	Thickness of clean layer
TQI	1.00	0.38	0.74	0.67	0.69	0.53	−0.29
Longitudinal level	0.38	1.00	−0.26	−0.24	0.68	0.64	−0.68
Alignment	0.74	−0.26	1.00	0.84	0.25	−0.04	0.12
Track gauge	0.67	−0.24	0.84	1.00	0.06	−0.11	0.05
Cross level	0.69	0.68	0.25	0.06	1.00	0.62	−0.35
Twist	0.53	0.64	−0.04	−0.11	0.62	1.00	−0.46
Thickness of clean layer	−0.29	−0.68	0.12	0.05	−0.35	−0.46	1.00

1. A negative value indicates a negative correlation between the two variables, while a positive value indicates a positive correlation. The larger the absolute value, the stronger the linear correlation.

$$\rho_{X,Y} = \frac{E[(X - \bar{X})(Y - \bar{Y})]}{\sigma_X \sigma_Y} \quad (5)$$

In the equation, E is the expected value; X and Y are the variables; \bar{X} and \bar{Y} are the mean values of the two variables; σ_X and σ_Y are the standard deviations of the two variables.

Table 1 presents the Pearson correlation coefficient between TQI factors and the thickness of the clean ballast layer. It reveals that the correlation coefficient between the thickness of the clean ballast layer and the longitudinal SD is -0.68 , which has the largest absolute value. This implies a relatively strong negative correlation between these two factors, while correlations with other factors are not as strong. Therefore, subsequent research in this paper primarily utilizes the longitudinal level to investigate its application in ballast layer inspection.

2.2. TDR calculation method

The indicator TDR is calculated using the standard deviation (SD) of the longitudinal level (vertical track irregularity) in a time series. The rationale behind choosing the track longitudinal level for TDR calculation was explained in Section 2.1. Track geometry data was collected by the Chinese comprehensive inspection train, which completes inspections twice a month. This enables the collection of long-term track geometry irregularity inspection data for the same section.

The change rate of the SD value of the longitudinal level is calculated as the indicator TDR (Equation 6), because the SD value of the longitudinal level increases with the deterioration of track geometry. Since the monthly inspection times were not fixed and each of the periods between two inspection times varied, to accurately calculate the indicator, monthly units were used, expressed as (mm/month).

$$TDR = \frac{\sum_{q=1}^{ns} (t_q - \bar{t})(s_q - \bar{s})}{\sum_{q=1}^{ns} (t_q - \bar{t})^2} \times 30 \quad (6)$$

In Equation 6, ns is the number of inspection data between two adjacent maintenance actions (details about the inspection data processing can be found in Section 2.3); t_q is the test date; s_q is the longitudinal level deviation values of the corresponding date; \bar{t} and \bar{s} are the mean values of t_q and s_q .

2.3. Longitudinal level data processing method

The longitudinal level data used for calculating TDR underwent two steps of processing, specifically data pre-processing and data segmentation, which are explained in this section. Notably, the longitudinal level data in this section is in a time series, which differs from the longitudinal data in the last section (in mileage series).

- The original inspected longitudinal level values are susceptible to interference from factors such as weather and equipment, so the outliers must first be removed.
- The back propagation (BP) method for the segmentation of time series is proposed and explained.

2.3.1. Data pre-processing

During the inspection of track geometry irregularities using an inspection train (under dynamic conditions), outliers may occur in the longitudinal level data (time series). Outliers appear as a significant deviation of the current test result from the results of adjacent tests, as shown in Figure 5a.

The median filtering method was applied to reduce the impact of these outliers on the longitudinal level data. Specifically, in an array of time series with multiple consecutive longitudinal levels for one railway-line section, a sliding window of size k is set. The size k means that the sample

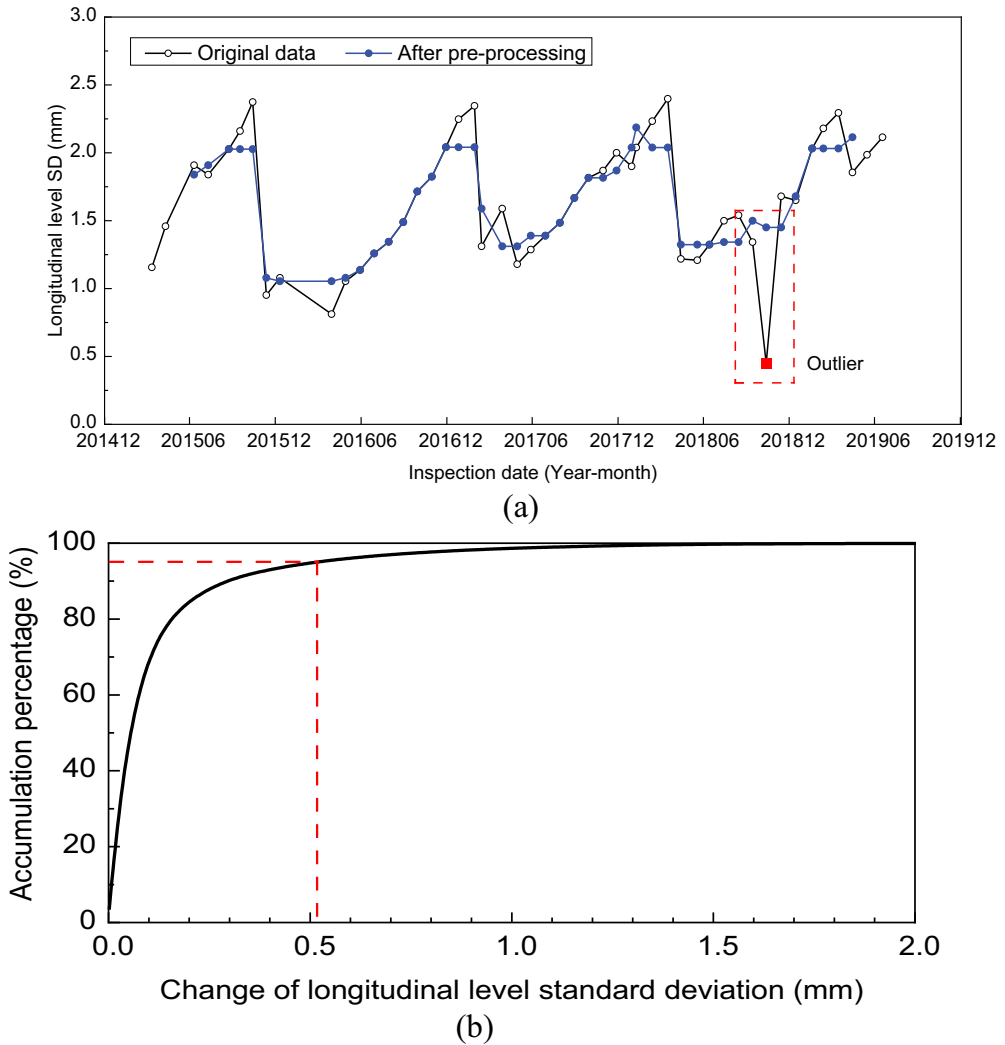


Figure 5. Data pre-processing method for longitudinal level SD: (a) Comparison of longitudinal level SD before and after median filtering method, (b) Change of two adjacent longitudinal level SDs in time series.

size in the window is k . The value for k was chosen as 5. This choice was made because k can be set as 3, 5, 7, ... and after multiple trials, it was found that data outliers are easily filtered out with a value of $k = 5$.

The window is slid from left to right in the array of time series, calculating the median of the k consecutive data in each window. When there is an outlier in the original sequence, the outlier shows a significant deviation from the median of the k consecutive data. Through this process, the outliers within this window are eventually identified and removed by setting a deviation threshold value. That is, if the deviation between a longitudinal level value and the median of the k consecutive data is larger than the threshold value, then this longitudinal level value is removed.

The threshold value was determined through probabilistic cumulative statistics on the change in longitudinal level of one railway line for two adjacent times, as shown in Figure 5b. From the figure, it can be seen that 95% of longitudinal level SD changes are smaller than 0.52 mm, so the threshold value was set as 0.5 mm.

2.3.2. Data segmentation

Data segmentation points (time series) of the longitudinal level are not fixed, which can cause traditional data segmentation methods to be inaccurate. A new segmentation method was developed to process data with different time series. This method is known as the back propagation segmentation method (BP method).

Over a period of time, track geometry irregularity can exceed the maintenance standard limits. After track geometry maintenance procedures, such as tamping and stabilization are performed, the track geometry immediately experiences a rapid change, followed by a slower, more gradual change (Figure 5a serves as an example).

$$f(t) = \begin{cases} a_1 t + b_1 & t < t_0 \\ a_2 t + b_2 & t \geq t_0 \end{cases} \quad (7)$$

In the equation, t is the variable, time; a_1 , a_2 , b_1 and b_2 are linear regression coefficients. Traditionally, Equation 7 shows the date segmentation of the longitudinal level SD in time series requires, which treats the duration the same value separated by the date segmentation points, t_0 .

While the intervals between two inspections may not always be consistent, the back-propagation (BP) method has been designed to handle this variance. This allows for the batch processing of date segmentation across different railway-line sections, creating efficiency and uniformity in the analysis process. The detailed steps of the BP method are illustrated in the flowchart shown in Figure 6.

The specific steps are introduced as follows:

Step 1. Each segment comprises left endpoints (LE) and right endpoints (RE). The goal of date segmentation in a time series is to identify the set of LE and RE. The set of all extreme points (E) in the entire time series is first established, thus creating subsets E, LE, and RE. The first element in set E is designated as the left endpoint L.

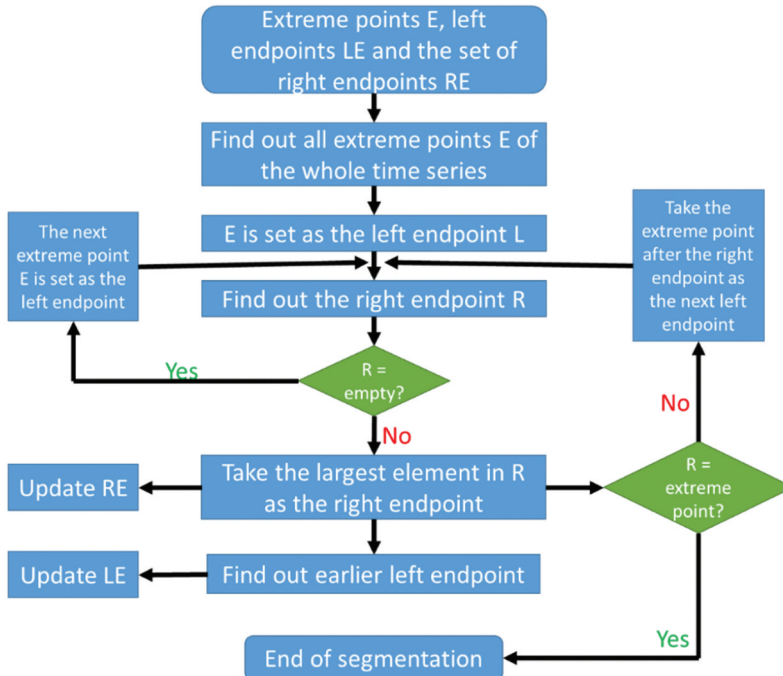


Figure 6. Flow chart of BP method for date segmentation of longitudinal level SD in time series.

Step 2. The right endpoint (R) is determined based on certain segmentation conditions, which include amplitude limits and time length limits among others. If R is empty, the next extreme point in set E is designated as the new left endpoint, and Step 2 is repeated until R becomes non-empty.

Step 3. The largest element in set R is assigned as the right endpoint. An extreme point is then found whose detection time is earlier than the right endpoint, whose amplitude is lower than the right endpoint, and whose segment length satisfies certain conditions. This extreme point becomes the new left endpoint. The sets LE and RE are updated accordingly. The extreme point following the right endpoint of this segment is selected as the next left endpoint, and the left endpoint is updated.

Step 4. Repeat Steps 2 and 3.

Step 5. To precisely locate each endpoint, the algorithm determines whether each element in the set of left endpoints (LE) and the set of right endpoints (RE) is an extreme value point. LE and RE are then updated based on this information.

3. Ballast layer health classification using TDR

3.1. TDR feature extraction

Several mixed passenger and freight railway lines (operating at speeds of 160–200 km/h) were chosen for this study, incorporating total track geometry data of a railway-line length of 2150 km. This equates to 10,500 effective railway-line sections. The track geometry irregularity data were collected by comprehensive inspection trains between January 2015 and September 2019, which were then used to extract the TDR features.

Figure 7 provides two examples of the TDR. It can be observed that the longitudinal level SD experiences periodic changes under the influence of maintenance operations.

Maintenance divides the data into separate cycles. Furthermore, within each cycle, the longitudinal level SD tends to increase in an approximately linear manner. It is worth noting that the TDR can be viewed as the slope of the SD of the longitudinal level within each cycle. The TDR values vary between cycles.

The study discovered that a sudden change in TDR between two adjacent cycles could indicate rapid degradation of the ballast layer. On this basis, we have defined the TDR feature as the difference between two consecutive TDRs.

Figure 8 depicts five typical TDR features, with each ‘P’ representing one feature and ‘t’ representing the inspection date. Five TDR features are proposed. It should be noted that these five TDR features have already been utilized and validated by field measurements and vision inspections (Section 4).

The principle behind using the TDR features to locate the railway-line section with ballast layer defects involves observing the change of TDRs in two adjacent cycles. For instance, if the line shape of the longitudinal level SD for one railway-line section resembles P1, it suggests that the ballast in this railway-line section is in good condition. P1 can also refer to the data from December 2014 to December 2016 in Figure 7a.

P1: TDRs in two adjacent cycles exhibit minor changes.

P2: The TDR suddenly increases on a specific date.

P3: Following maintenance, the TDR becomes smaller than the TDR in the previous cycle.

P4: The longitudinal level SD continues to increase after maintenance, and the TDR undergoes little change.

P5: The TDR is significantly larger than other cycles, as well as TDRs in other adjacent railway-line sections.

Based on the TDR features, we propose the Ballast Layer Health Classification (BLHC), which can quickly identify railway-line sections with defects or impending defects. As depicted in Table 2,

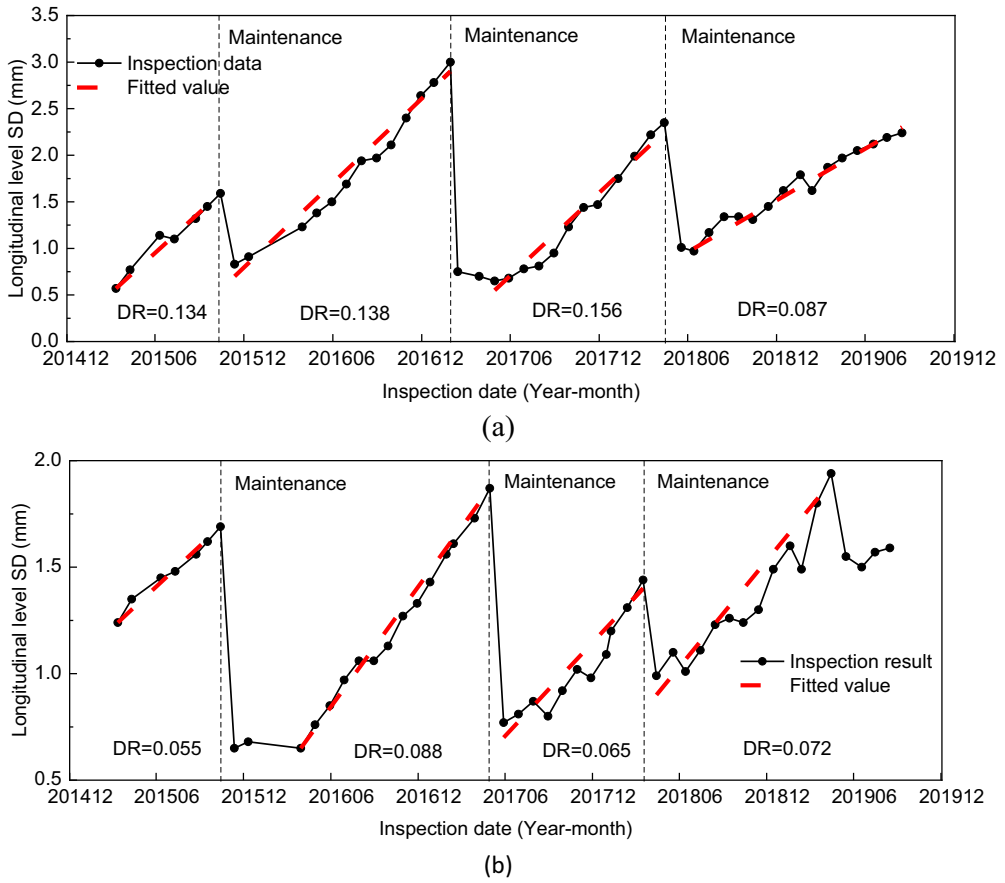


Figure 7. Two examples of longitudinal level SD to feature TDR: (a) Railway line section #1, (b) Railway line section #2.

a classification of $C = 2$ and $C = 5$ indicates that the ballast layer is likely to develop defects in the near future.

In the following sections, we'll explain why we chose the magnitude of TDR as the indicator for possible ballast layer defects. More specifically, for example, we'll address why 'TDR exceeds 0.1 mm/month' is considered a significant value for BLHC (as shown in Table 2). In summary, we extracted the TDR features by processing the TDR data of 5000 railway-line sections and then analysed the distribution pattern (probability density distribution) of these data to finally establish the BLHC criteria.

3.2. TDR feature distribution pattern

Because the $C = 2$ and $C = 5$ are the indicators, predicting possible ballast layer defects, for which how the TDR value thresholds were chosen is explained.

3.2.1. Feature analysis for obtaining classification 5 ($C = 5$)

Through the track geometry data of 5000 different railway-line sections, diverse TDRs were obtained. To guarantee the diversity of the TDRs, operating lines under various field conditions were selected to capture all kinds of TDRs. These TDRs were suitable for obtaining the distribution pattern of the TDRs. Based on the distribution pattern of the TDRs, the BLHC can be made more reliable and applicable for ballast layer health monitoring.

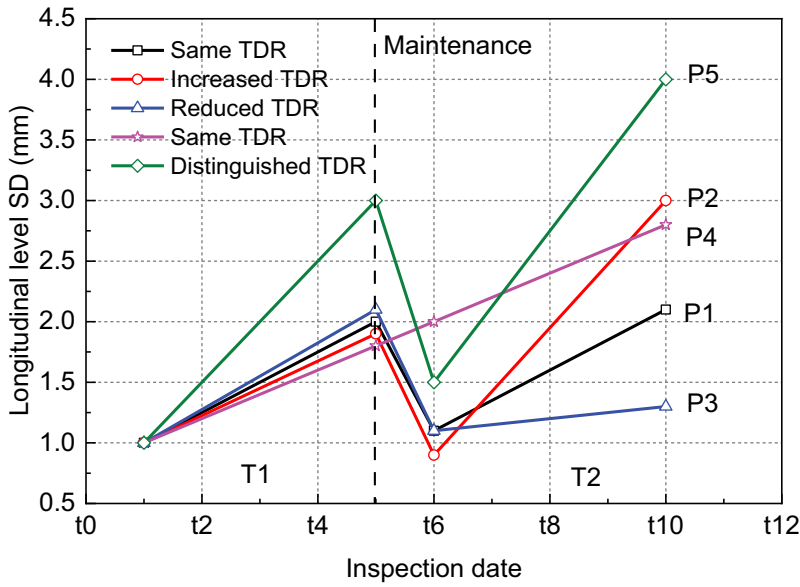


Figure 8. Illustration of five typical TDR features.

Table 2. Ballast layer health classification using TDR features.

Classification	Name	TDR features	Railway line health condition
C=1	Normal periodic deterioration	No significant changes in TDR gradient compared to the previous cycle, and the TDR value is relatively small	Line quality in good condition
C=2	Abrupt deterioration	The TDR gradient has changed abruptly compared to the previous TDR gradient, and the difference exceeds 0.05 mm/month	Possible upcoming defects
C=3	Effective maintenance	After maintenance, the TDR gradient becomes smaller and the TDR values are small.	Line quality in good condition
C=4	Deterioration rising	A continuous or fluctuating rise in TDR value, $0 < \text{TDR} < 0.1$	Ballast layer continues on degradation
C=5	Severe deterioration	In the same degradation cycle, the TDR gradient of this section is much greater than the TDR gradient of adjacent cycles as well as gradient of other adjacent sections and the TDR exceeds 0.1 mm/month .	Possible upcoming defects

The probability density of the TDRs was fitted with a lognormal distribution function, and the fitting formula is given in Equation 8 [43]. The goodness-of-fit R^2 is used to evaluate the efficacy of the fit, as shown in Equation 9 [44].

$$f(TDR, \mu_{TDR}, \sigma_{TDR}) = c_0 + \frac{A}{\sqrt{2\pi}TDR\sigma_{TDR}} e^{-\frac{(\ln TDR - \mu_{TDR})^2}{2\sigma_{TDR}^2}} \quad (8)$$

$$R^2 = \frac{\sum_{i=1}^B (\hat{P}OD_i - \bar{P}OD)^2}{\sum_{i=1}^B (POD_i - \bar{P}OD)^2} \quad (9)$$

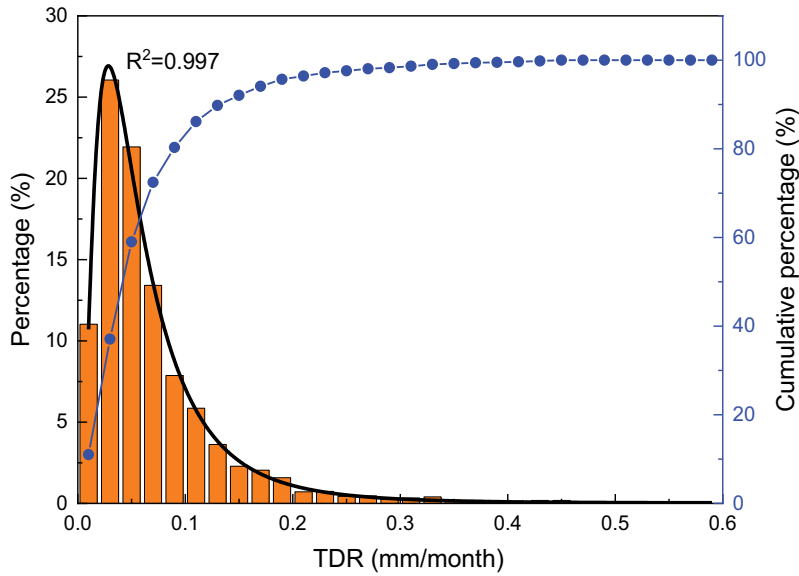


Figure 9. Statistical graph of TDR.

Table 3. Parameters for fitting distribution of TDR.

Parameter	c_0	A	μ_{TDR}	σ_{TDR}	R^2
Fitted value	0.027	1.98	0.051	0.769	0.997

In the equation, c_0 and A are two constants; μ_{TDR} and σ_{TDR} are the mean and SD of the logarithm of the variable, respectively; POD_i is the actual probability density; \bar{POD} is the mean probability density; \hat{POD}_i is the fitted probability density; R^2 is the goodness of fit.

The results of the TDR probability density distribution are shown in Figure 9, indicating that the TDR primarily ranges between 0.02 and 0.08 mm/month. The goodness-of-fit R^2 is 0.997, demonstrating clear log-normal distribution characteristics. The specific fitting parameters are presented in Table 3.

The TDR values outside the normal range require attention because, based on maintenance experience with railway lines, locations with abnormal TDRs have a higher likelihood of defect occurrence. The normal range of the TDR was ultimately set between 0 and 0.1 mm/month. Initially, using a 90% confidence interval, the normal range of the TDR was calculated to be between 0 and 0.13 mm/month. However, considering that the quality of the ballast layer varies across different lines, causing variations in TDR values, the range was adjusted to 0–0.1 mm/month to avoid overlooking sections with potential ballast layer defects. In other words, any sections with a TDR exceeding 0.1 mm/month should be monitored more closely for potential degradation.

3.2.2. Feature analysis for obtaining classification 2 ($C = 2$)

The Classification 2 ($C = 2$) was obtained by measuring the changes in TDR during different degradation cycles for the same section. Dispersion indicators were used for quantitative analysis. As demonstrated in Figure 7a,b the mean values of the TDR in different sections vary, making direct comparisons of their standard deviations (SDs) impractical. As such, the Coefficient of Variation (CV) was employed to compare the changes in TDR across different degradation cycles for the same section [45]. The CV is the ratio of the SD to the mean, which can eliminate the influence of

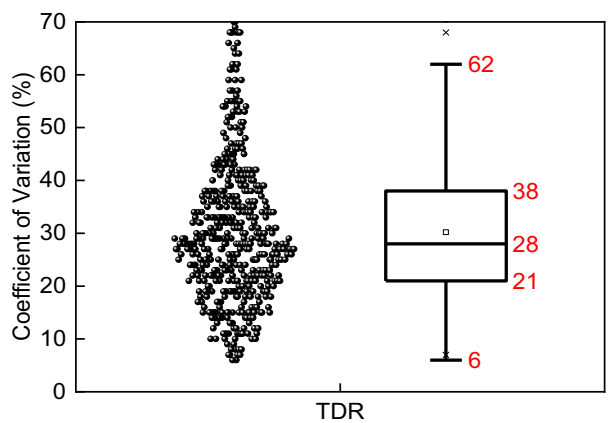


Figure 10. Coefficient of variation for TDR.

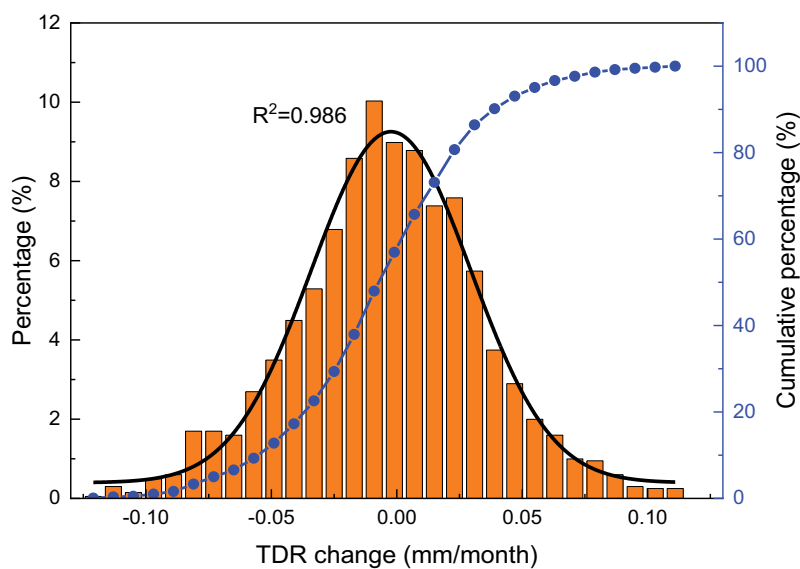


Figure 11. Statistical graph of the TDR difference in each adjacent two degradation cycles.

Table 4. Parameters for fitting distribution of TDR change.

Parameter	$\mu_{\Delta TDR}$	$\sigma_{\Delta TDR}$	R^2
Fitted value	0	0.028	0.986

different mean values on the comparison of multiple degrees of variation. A low CV value indicates low dispersion, as shown in Equation 10. In this equation, σ represents the SD and μ represents the mean value.

$$CV = \frac{\sigma}{\mu} \times 100\% \tag{10}$$

The CVs for the TDR of each railway-line section were computed for statistical analysis and are illustrated in Figure 10. The median CV displayed in the graph is 28%, and half of the CVs in the

sample fall between 21% and 38%. This suggests that the dispersion in the TDR across the railway-line sections is relatively uniform and minor.

The TDR for the same railway section displays minor dispersion, yet there still exists a certain difference in the TDR of adjacent degradation cycles. For a quantitative analysis of the TDRs in two consecutive degradation cycles, data from 5000 railway-line sections (spanning two adjacent degradation cycles) were statistically analysed. The results, presented in Figure 11, demonstrate that the differences in TDR across each pair of adjacent cycles follow a normal distribution.

The fitting formula is provided in Equation 11 [46], with the parameters for the normal distribution given in Table 4. The goodness-of-fit R^2 reached 0.986, indicating that the assumption of a normal distribution is valid. This suggests that the variability of the TDR change follows a normal distribution. According to the cumulative percentage of TDR change, the maximum value of the TDR change under a 90% confidence interval is calculated to be 0.05 mm/month.

$$f(\mu_{\Delta TDR}, \sigma_{\Delta TDR}) = \frac{A}{\sqrt{2\pi}\sigma_{\Delta TDR}} e^{-\frac{(\Delta TDR - \mu_{\Delta TDR})^2}{2\sigma_{\Delta TDR}^2}} \quad (11)$$

4. Field validation for TDR and BLHC

4.1. Correlation of TDR and ballast layer fouling index

Earlier studies have demonstrated that the scattering characteristics of Ground Penetrating Radar (GPR) waves can be used to ascertain the porous structure of ballast layers. It has been proven that there is a strong correlation between the GPR-based fouling index (calculated based on radar detection data) and the actual fouling level of the ballast layer [4,23,47]. This suggests that GPR can effectively reflect the health condition of the ballast layer.

In this study, we employed GPR inspection data of the ballast layer to validate the TDR. The GPR inspection methodology and signal processing means can be found in the authors' previous publications [4,47]. We compared the GPR-based fouling index with the TDR, as shown in Figure 12.

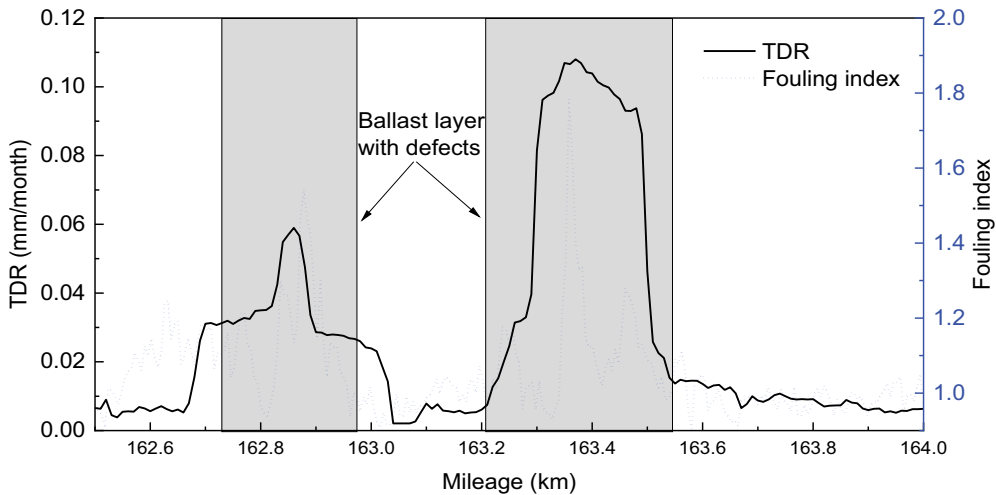


Figure 12. Correlation between TDR and GPR-based fouling index.

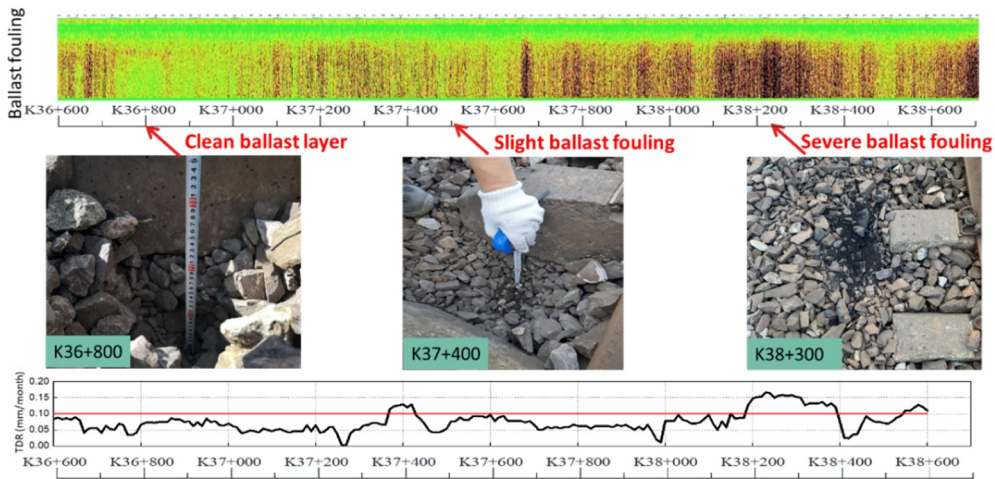


Figure 13. GPR-based fouling index, field conditions and TDR.

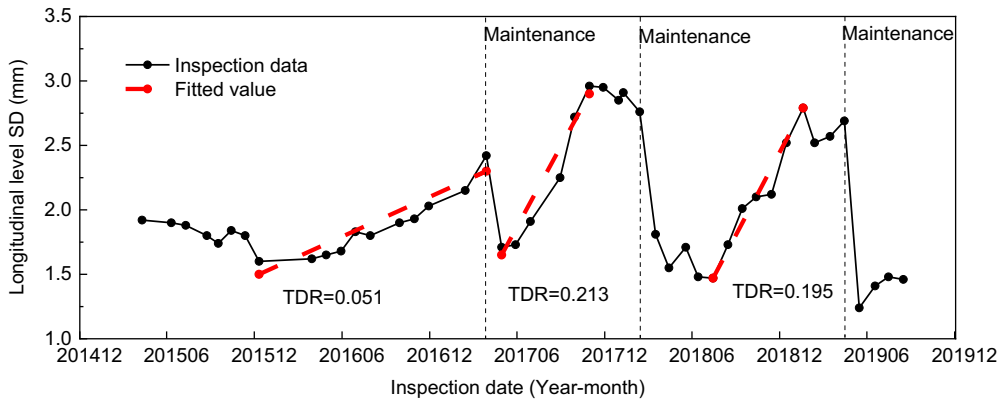
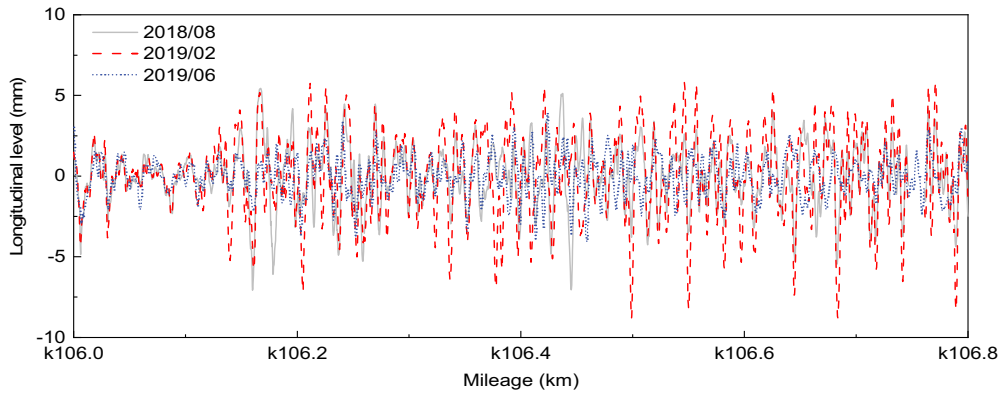


Figure 14. Longitudinal level SD of section near K106+300.

From the figure, it is evident that sections with high TDR values also exhibit a high fouling level (as inspected by GPR). In nearly all cases, a ballast layer with high fouling levels also shows severe ballast degradation. Furthermore, fouled ballast layers usually lead to rapid track irregularity degradation. Therefore, when the TDR value is high, the track can be identified as requiring maintenance. Ultimately, combining these two types of ballast layer inspection methods (GPR and inspection train) provides a more precise method for ballast layer health inspection and monitoring.

Upon identifying this correlation, further validations were carried out in field tests, as depicted in Figure 13. Specifically, a 2 km railway line section (section mileage: K36 + 600 – K38 + 600) was selected for the case study. The TDR, GPR fouling index, and field ballast layer condition (ascertained by digging a hole) for the same section were compared, as shown in Figure 13. In the GPR detection figure, the black colour indicates a high fouling level.

From the figure, it can be observed that the section near K36 + 800 has a low ballast layer fouling level, while the section from K38 + 200 to K38 + 400 has a high ballast layer fouling level. Accordingly, the TDR values in these sections correlate with the fouling level (K36 + 800: low TDR; K38 + 200 - K38 + 400: high TDR).



(a)



(b)

Figure 15. Ballast layer condition of railway line section near K106.300: (a) Raw longitudinal level data of section near K106.300, (b) Ballast layer condition (mud-pumping, high fouling level).

4.2. Ballast layer health classification validation

In the first case study, the railway-line section near K106 + 300 was selected due to suspicion of a ballast layer defect, as its BLHC was rated as $C = 5$. The longitudinal level SD and corresponding TDR values are shown in Figure 14. The following explanations are provided, with further details on the BLHC found in Table 2. For $C = 5$: the TDR measures 0.213 and 0.195 mm/month, both of which exceed the threshold value of 0.1 mm/month.

The inspected raw longitudinal level data (obtained from the inspection train) of the section K106 + 200 - K106 + 400 was examined (see Figure 15a), which shows a significant increase in the longitudinal level value along with the inspection date. This validates the sensitivity and accuracy of the TDR. Moreover, the application of TDR was corroborated by the distinct mud-pumping phenomenon evident in this section (see Figure 15b).

In the second case study, the railway-line section near K17 + 700 was analysed due to the suspected ballast layer defects with a BLHC of $C = 5$. The longitudinal level SD and TDR of the section near K17 + 700 are shown in Figure 16a. It is evident from the figure that the TDR surpassed the threshold value of 0.1 mm/month and is notably higher than the TDR values of the two adjacent sections (Figure 16b/c).

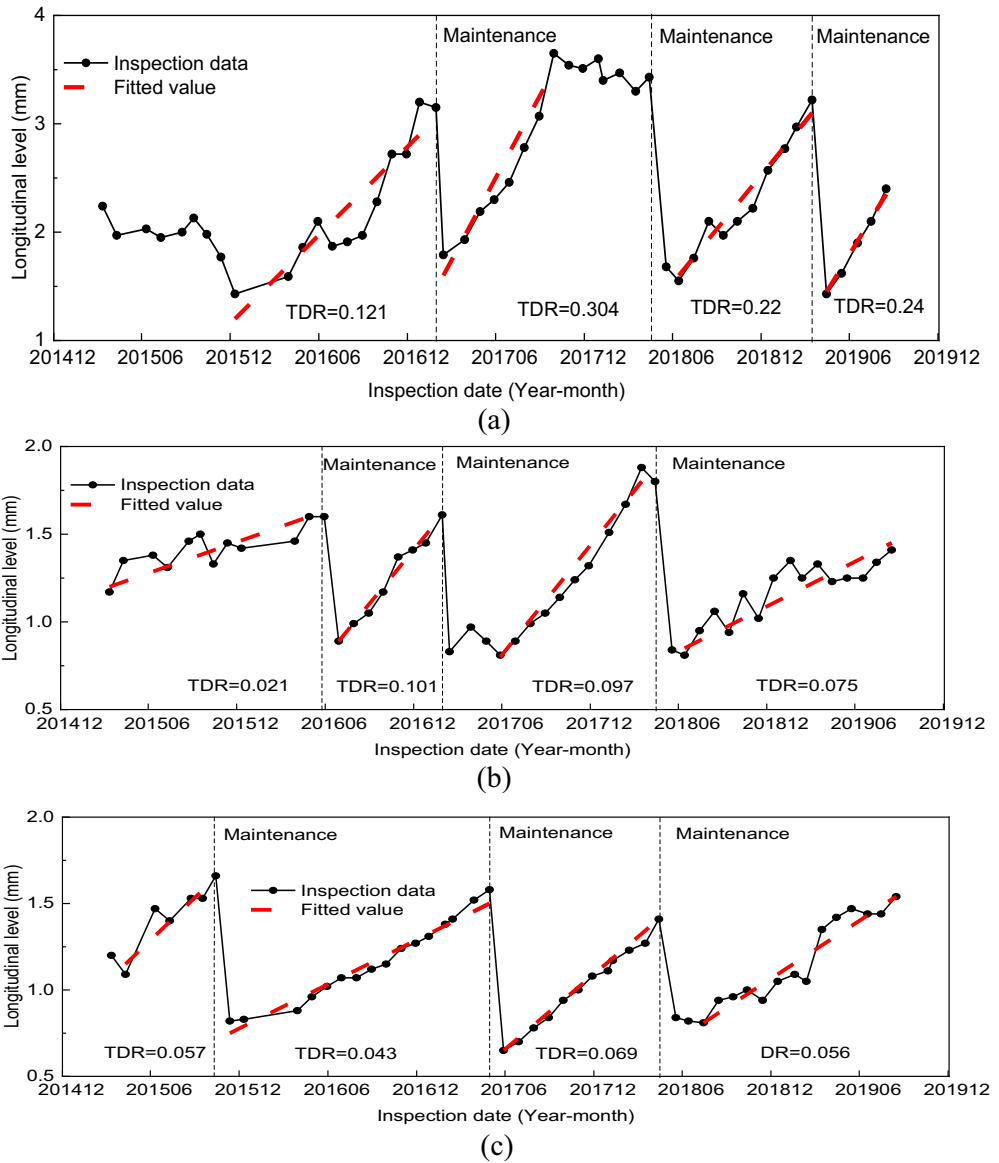


Figure 16. Longitudinal level SD and TDR of railway line section near K17+700: (a) Longitudinal level and TDR of railway line section at K17+700, (b) Longitudinal level and TDR of railway line section at K17+500, (c) Longitudinal level and TDR of railway line section at K18+000.

Based on the longitudinal level and TDR results, the railway-line section at L17 + 700 was inspected in the field. The condition of the ballast layer is shown in Figure 17. It is evident that the ballast particles have undergone significant crushing, resulting in a detrimental impact on the bearing capacity of the ballast layer and the ride comfort of the track. Consequently, it is recommended to renew the ballast layer in this section.

From Figures 16 and 17, it is evident that the TDR values in railway sections with ballast layer defects exhibit significant changes, whereas in the neighbouring sections without defects, the TDR changes are relatively small and stable. This observation underscores the effectiveness of using TDR as a tool for identifying ballast layer defects.



Figure 17. Ballast layer in the field at railway line section K17+700.

5. Conclusions

In this study, a new method called the back propagation segmentation method was proposed to process track geometry data and establish a new indicator called the track degradation rate (TDR) for identifying ballast layer defects. The TDR was calculated based on the track geometry irregularity represented by the longitudinal level standard deviation (SD), and statistical analysis was performed on 5000 railway-line sections to evaluate the condition of the ballast layer through the TDR.

The main conclusions of this study are as follows:

- (1) There is a relationship between track geometry irregularity and the ballast layer condition, particularly a significant negative correlation between the longitudinal level SD and the thickness of the clean ballast layer.
- (2) The longitudinal level exhibits a periodic deterioration trend, and the trend is approximately linear within the same period/cycle. The TDR variation coefficient is generally within 30%. The maximum TDR value within the 90% confidence interval is 0.1 mm/month, and the maximum TDR change compared to adjacent periods is 0.05 mm/month.
- (3) Based on the characteristics of TDR changes, the ballast layer conditions are classified into five classes: normal periodic deterioration, abrupt deterioration, effective maintenance, deterioration rising, and severe deterioration. The classification was validated by reviewing railway-line sections with severe deterioration.

The comparison between the TDR-BHLC evaluation and field measurements demonstrates that this method can effectively identify sections with serious ballast layer deterioration. These findings contribute to the understanding and assessment of ballast layer conditions in railway tracks.

The TDR and BLHC indicators proposed in this study have the potential to facilitate the health monitoring and evaluation of ballast layers, providing valuable support for maintenance decisions in ballasted tracks. The next steps in this research will focus on refining the evaluation method to enhance its accuracy and reliability. This refinement process will involve incorporating specific field maintenance practices and historical data to further improve the effectiveness of the evaluation.

Furthermore, the BLHC classification can efficiently identify the locations of ballast layer defects. This information can be combined with ground penetrating radar (GPR) inspections to

analyse the underlying reasons for these defects. Ongoing research is underway to establish correlations between the ballast layer fouling index, TDR values, and GPR inspection results. By integrating these different inspection techniques, a comprehensive understanding of the ballast layer condition can be achieved, enabling more informed decision-making and targeted maintenance strategies.

Acknowledgements

This research is funded by the Key Research and Development Project of the China Academy of Railway Sciences Corporation Limited (2021YJ251), the China national special project for the development of major research instruments and equipment under grant 52027813. The European Commission and UKRI Engineering and Physical Science Research Council (EPSRC) are acknowledged for the Re4Rail project (Grant No EP/Y015401/1).

Disclosure statement

No potential conflict of interest was reported by the author(s).

ORCID

Yunlong Guo  <http://orcid.org/0000-0003-4339-1833>

References

- [1] Indraratna B, Salim W, Rujikiatkamjorn C. Advanced rail geotechnology: ballasted track. CRC press London: 2011. doi:10.1201/b10861
- [2] Li D, Hyslip J, Sussmann T, et al. Railway geotechnics. CRC Press; 2015.
- [3] Guo YL, Zong L, Markine V, et al. Experimental and numerical study on lateral and longitudinal resistance of ballasted track with nailed sleeper. *Int J Rail Transp.* 2022;10(1):114–132. DOI:10.1080/23248378.2021.1872424
- [4] Guo YL, Liu GX, Jing GQ, et al. Ballast fouling inspection and quantification with ground penetrating radar (gpr). *Int J Rail Transp.* 2023;11(2):151–168. DOI:10.1080/23248378.2022.2064346
- [5] Tutumluer E, Qian Y, Hashash YMA, et al. Discrete element modelling of ballasted track deformation behaviour. *Int J Rail Transp.* 2013;1(1–2):57–73. DOI:10.1080/23248378.2013.788361
- [6] Shi C, Fan Z, Connolly DP, et al. Railway ballast performance: recent advances in the understanding of geometry, distribution and degradation. *Transp Geotech.* 2023;41:101042. DOI:10.1016/j.trgeo.2023.101042
- [7] Liu SS, Huang H, Qiu T, et al. Comparison of laboratory testing using smartrock and discrete element modeling of ballast particle movement. *J Mater Civil Eng.* 2017;29(3):D6016001. DOI:10.1061/(ASCE)MT.1943-5533.0001540
- [8] Danesh A, Palassi M, Mirghasemi AA. Evaluating the influence of ballast degradation on its shear behaviour. *Int J Rail Transp.* 2018;6(3):145–162. doi: 10.1080/23248378.2017.1411212
- [9] Rohrman AK, Ho CL. Effects of fouling containing plastic fines on abraded ballast strength and deformation properties. *Transp Geotech.* 2019;21:100278. doi: 10.1016/j.trgeo.2019.100278
- [10] Tennakoon N, Indraratna B, Rujikiatkamjorn C, et al. The role of ballast-fouling characteristics on the drainage capacity of rail substructure. *Geotech Test J.* 2012;35(4):629–640. DOI:10.1520/GTJ104107
- [11] Selig ET, Waters JM. Track geotechnology and substructure management. Thomas Telford Publishing; 1994. doi:10.1680/tgasm.20139
- [12] Huang H, Moaveni M, Schmidt S, et al. Evaluation of railway ballast permeability using machine vision-based degradation analysis. *Transp Res Rec.* 2018;2672(10):62–73. DOI:10.1177/0361198118790849
- [13] Indraratna B, Singh M, Nguyen TT. The mechanism and effects of subgrade fluidisation under ballasted railway tracks. *Railw Eng Sci.* 2020;28(2):113–128. doi: 10.1007/s40534-020-00210-1
- [14] Kuo CP. Ground-penetrating radar to investigate mud pumping distribution along a railway line. *Constr Build Mater.* 2021;290:123104. doi: 10.1016/j.conbuildmat.2021.123104
- [15] Barbosa JMD, Faragau AB, van Dalen KN, et al. Modelling ballast via a non-linear lattice to assess its compaction behaviour at railway transition zones. *J Sound Vib.* 2022;530:116942. DOI:10.1016/j.jsv.2022.116942
- [16] Sysyn M, Nabochenko O, Kovalchuk V. Experimental investigation of the dynamic behavior of railway track with sleeper voids. *Railw Eng Sci.* 2020;28(3):290–304. doi: 10.1007/s40534-020-00217-8

- [17] Qian Y, Mishra D, Tutumluer E, et al. Characterization of geogrid reinforced ballast behavior at different levels of degradation through triaxial shear strength test and discrete element modeling. *Geotext Geomem.* 2015;43(5):393–402. DOI:10.1016/j.geotextmem.2015.04.012
- [18] Indraratna B, Tennakoon N, Nimbalkar S, et al. Behaviour of clay-fouled ballast under drained triaxial testing. *Geotechnique.* 2013;63(5):410–419. DOI:10.1680/geot.11.P.086
- [19] Akagawa S, Hori M, Sugawara J. Frost heaving in ballast railway tracks. *Procedia Engineer.* 2017;189:547–553. doi: 10.1016/j.proeng.2017.05.087
- [20] Nguyen TT, Indraratna B. Rail track degradation under mud pumping evaluated through site and laboratory investigations. *Int J Rail Transp.* 2021;10(1):44–71. doi: 10.1080/23248378.2021.1878947
- [21] Mishra D, Boler H, Tutumluer E, et al. Deformation and dynamic load amplification trends at railroad bridge approaches effects caused by high-speed passenger trains. *Transp Res Rec.* 2017;2607(1):43–53. DOI:10.3141/2607-07
- [22] Lamas-Lopez F, Cui YJ, Calon N, et al. Track-bed mechanical behaviour under the impact of train at different speeds. *Soils Found.* 2016;56(4):627–639. DOI:10.1016/j.sandf.2016.07.004
- [23] Wang S, Liu G, Jing G, et al. State-of-the-art review of ground penetrating radar (gpr) applications for railway ballast inspection. *Sensors.* 2022;22(7):2450. DOI:10.3390/s22072450
- [24] Goodarzi S, Kashani HF, Saeedi A, et al. Stochastic analysis for estimating track geometry degradation rates based on gpr and lidar data. *Constr Build Mater.* 2023;369:130591. DOI:10.1016/j.conbuildmat.2023.130591
- [25] Bianchini Ciampoli L, Gagliardi V, Clementini C, et al. Transport infrastructure monitoring by insar and gpr data fusion. *Surv Geophys.* 2019;41(3):371–394. DOI:10.1007/s10712-019-09563-7
- [26] Barrett BE, Day H, Gascoyne J, et al. Understanding the capabilities of gpr for the measurement of ballast fouling conditions. *J Appl Geophys.* 2019;169:183–198. DOI:10.1016/j.jappgeo.2019.07.005
- [27] De Bold R, O'Connor G, Morrissey JP, et al. Benchmarking large scale gpr experiments on railway ballast. *Constr Build Mater.* 2015;92:31–42. DOI:10.1016/j.conbuildmat.2014.09.036
- [28] Guler H, Jovanovic S, Evren G. Modelling railway track geometry deterioration. *Proc Instit Civil Engin Trans.* 2011;164(2):65–75. doi: 10.1680/tran.2011.164.2.65
- [29] Dahlberg T. Some railroad settlement models—a critical review. *Proc Inst Mech Eng F J Rail Rapid Transit.* 2001;215(4):289–300. doi: 10.1243/0954409011531585
- [30] Liao Y, Han L, Wang H, et al. Prediction models for railway track geometry degradation using machine learning methods: a review. *Sensors.* 2022;22(19):7275. DOI:10.3390/s22197275
- [31] Nielsen JCO, Berggren EG, Hammar A, et al. Degradation of railway track geometry – correlation between track stiffness gradient and differential settlement. *Proc Inst Mech Eng F J Rail Rapid Transit.* 2018;234(1):108–119. DOI:10.1177/0954409718819581
- [32] Abadi T, Le Pen L, Zervos A, et al. A review and evaluation of ballast settlement models using results from the Southampton railway testing facility (srft). *Advan Transport Geotech.* 2016;143:999–1006. DOI:10.1016/j.proeng.2016.06.089
- [33] Esveld C. Modern railway track. Vol. 385. The Netherlands: MRT-productions Zaltbommel; 2001.
- [34] Vale C, Ribeiro IM, Calçada R. Integer programming to optimize tamping in railway tracks as preventive maintenance. *J Transp Eng.* 2012;138(1):123–131. doi: 10.1061/(ASCE)TE.1943-5436.0000296
- [35] Khajehei H, Ahmadi A, Soleimanmeigouni I, et al. Prediction of track geometry degradation using artificial neural network: a case study. *Int J Rail Transp.* 2022;10(1):24–43. DOI:10.1080/23248378.2021.1875065
- [36] Luo L, Zhang G, Wu W, et al. Control of track irregularity of wheel-rail system. China Beijing: China Railway Publishing House; 2006.
- [37] Standard B Railway applications/track-track geometry quality.
- [38] Guo YL, Markine V, Jing GQ. Review of ballast track tamping: mechanism, challenges and solutions. *Constr Build Mater.* 2021;300:123940. doi: 10.1016/j.conbuildmat.2021.123940
- [39] Kashani HF, Ho CL, Hyslip JP. Fouling and water content influence on the ballast deformation properties. *Constr Build Mater.* 2018;190:881–895. doi: 10.1016/j.conbuildmat.2018.09.058
- [40] Indraratna B, Ngo NT, Rujikiatkamjorn C. Behavior of geogrid-reinforced ballast under various levels of fouling. *Geotext Geomem.* 2011;29(3):313–322. doi: 10.1016/j.geotextmem.2011.01.015
- [41] Esmaeili M, Aela P, Hosseini A. Experimental assessment of cyclic behavior of sand-fouled ballast mixed with tire derived aggregates. *Soil Dyn Earthquake Eng.* 2017;98:1–11. doi: 10.1016/j.soildyn.2017.03.033
- [42] Liu GX, Peng Z, Jing GQ, et al. Railway ballast layer inspection with different gpr antennas and frequencies. *Transp Geotech.* 2022;36:100823. DOI:10.1016/j.trgeo.2022.100823
- [43] Devore JL. Probability and statistics for engineering and the sciences. London, United Kingdom: Cengage learning; 2011.
- [44] Gerbing DW, Anderson JC. Monte-carlo evaluations of goodness of fit indexes for structural equation models. *Sociol Method Res.* 1992;21(2):132–160. doi: 10.1177/0049124192021002002
- [45] Abdi H. Coefficient of variation. In: Neil, S, editors. Encyclopedia of research design. Vol. 1. J Thousand Oaks, CA: SAGE Publications; 2010. pp. 170–172.

- [46] Magnus JR. Estimation of the mean of a univariate normal distribution with known variance. *Econom J.* 2002;5(1):225–236. doi: [10.1111/1368-423X.t01-1-00082](https://doi.org/10.1111/1368-423X.t01-1-00082)
- [47] Guo YL, Wang SL, Jing GQ, et al. Assessment of ballast layer under multiple field conditions in china. *Constr Build Mater.* 2022;340:127740. DOI:[10.1016/j.conbuildmat.2022.127740](https://doi.org/10.1016/j.conbuildmat.2022.127740)